Microstructure, oxidation resistance and mechanical properties of stellite 12 composite coating doped with submicron TiC / B_4C by laser cladding

Qiran Cheng[1,2],Haichuan Shi[1,2 *],Peilei Zhang[1,2],Zhishui Yu[1,2],Wudi[1,2],Shanshan He[1,2] and Yingtao Tian[3]

1. School of Materials Engineering, Shanghai University of Engineering Science, Shanghai 201620, China;
2. Shanghai Collaborative Innovation Center of Laser Advanced Manufacturing Technology, Shanghai 201620, China;
3. Department of Engineering, Lancaster University, Bailrigg, Lancaster, LA1 4YW, United Kingdom;

ABSTRACT:

Stellite 12 and Ti/B_4C composite coatings were successfully fabricated on the surface of 304 stainless steel substrates by laser cladding. The effect of Ti/B_4C with different mass fractions on the structure and properties of Stellite 12 coating were studied. The properties and the growth mode of the coating were analyzed. The results show that the Stellite 12 coating was mainly composed of face-centered cubic γ-Co and Cr_7C_3. With the addition of Ti/B_4C, TiC submicron particle phase was synthesized in situ in the coatings. Residual B_4C as a heterogeneous nucleus particle, forming a submicron microstructure TiC/B_4C strengthening phase, and the particle size gradually decreases. The TiC/B_4C particles can refine the grains of the coatings. The micro-hardness of the coating gradually increased with the increase of Ti/B_4C, and the highest were 650HV. The wear resistance and oxidation resistance of the coatings gradually increased with the increase of Ti/B_4C.

1.Introduction

Nowadays, stainless steel is used in many industrial scenes, but it still has some problems in different actual conditions, such as: low hardness, high coefficient of friction, and poor wear resistance. These disadvantages will reduce the service life of mechanical parts. Not only that, but it will have a great impact on the reliability of mechanical parts and components, and will eventually cause serious economic losses. Now there is a new way of surface strengthening. The laser-coated Co-based cemented carbide composite coatings were used to improve the performance of stainless steel. Compare with Ni-based and Fe-based surface hardening alloys, Co-based hardening alloys are more suitable for protecting aerospace gas turbines and

* Corresponding author at: Room 3109, School of Materials Engineering, 333 Long Teng Rd. Songjiang Campus of Shanghai University of Engineering Science, Shanghai, 201620, China. Tel: +86 19802109520; Fax: +86 21 67791377. Email addresses: shc0010@126.com (Haichuan Shi).

power plants[1]. Stellite alloy is the most popular hard alloy in Co-based alloys. It also contains a hard phase in the lower eutectic or solid solution matrix, which can be used in non-lubricated wear conditions[2]. Stellite 12 (1.6% C mass fraction) is a surface hardening alloy between Stellite 6 and Stellite 1. Stellite 12 is becoming increasingly popular for wear-resistant applications. Although the Stellite 12 coating shows excellent overall performance in the application of engineering parts, but the wear resistance is still a problem, especially under high temperature environment or heavy load, its service life will be greatly reduced[3].

Laser cladding is a rapid melting and nonequilibrium solidification process. And it can form a good metallurgical bond between the substrate and the coating.[4] In recent years, with the development of laser technology, laser cladding, laser fusion, laser quenching and other emerging laser technology has emerged. Feng et al. [5] used laser coating technology to prepare Ni-Cr and Al_2O_3 composite coatings on the surface of stainless steel. Kwok and Pan's [6][7] found that the pitting corrosion resistance, crevice corrosion and intergranular corrosion resistance of the stainless steel had greatly improved after laser surface melting treatment. Yang et al. [8] successfully prepared Co-based coatings by laser welding with dense microstructure without any microcracks and pores. But there were some problems with the Co-base alloy coating. The wear resistance of the Co-based alloy coatings is poor. A hard phase needs to be added to the Co-based alloy to improve wear resistance before it can be used in the actual manufacturing process. In Co-based carbide, Stellites developed as Co,Cr,W,C type were the most popular group[9][10] that can be found in several modifications and commercial grades such as Stellite 1, 6 and 12. [11] The main factor that distinguishes these classifications is carbon content. The difference in carbon content results a different amount of carbide in the microstructure, which changes the hardness. [9][12] A. Gholipour et al. [1] analyzed the microstructure and mechanical properties of laser cladding Stellite 6 coating on 17-4ph stainless steel. Compared with the base material, the microhardness of the coating increased a little, but the wear resistance and corrosion resistance became worse. In the study of A. sihroozi et al. [13], they found that adding Ti and C can form a compound with Co. The presence of this compound can refine the coating grains and improve its micro-hardness and wear resistance. Zhu et al. [14] studied the doping of Ti/B_4C in stellite 6 to improve the performance of the coating. TiC and TiB phases were formed in the coating to improve the micro-hardness and wear resistance of the coating. Du et al. [15] studied the addition of Ti and B_4C powders to iron-based powders. During the laser welding process, Fe and B_4C were used as precursors to form TiB_2 and TiC in situ. Compared with direct addition, the product obtained in this way was smaller and more dispersed. This was more conducive to refine the structure, improve the mechanical properties of the coating. According to previous studies, adding Ti/B_4C to Stellite alloys to form a composite coating is a promising method of coating strengthening. In this way, TiB and TiC phases can be generated in situ in the coating to improve coating performance. At the same time, stelite 12 has the most balanced mechanical properties due to its moderate carbon content in all Stellite alloys. [16][17] Therefore, the advantages of both can be combined to prepare the composite coatings

by laser cladding.

In this paper, Stellite 12 coating and Stellite 12+Ti/B_4C (2%,4%,6%,8%) composite coatings were prepared on the surface of 304 stainless steel by laser cladding. The polycrystalline X-ray diffractometer (XRD) and scanning electron microscope (SEM) were used to analyze the coating phase and microstructure, and the wear resistance at room temperature and oxidation resistance at high temperature were also tested.

2. Materials and Methods

2.1Materials

In this study, the substrate was 304 stainless steel with the dimensions of 50 mm × 50 mm × 10 mm. Before laser cladding, the cladding surface was abraded and then cleaned ultrasonically with alcohol. The chemical composite of the substrates is listed in Table 1.

Table 1. Chemical composition of 304 stainless steel (wt %)

Fe	C	Si	Mn	P	S	Cr	Ni
Bal	≤0.08	≤1	≤2	≤0.035	≤0.03	18-20	8-10.5

The chemical composite of the powders are listed in Table 2. Ti/B_4C powders with a mass fraction of 2%, 4%, 6%, 8% were added to the Stellite 12 powders, in which the ratio of Ti to B_4C powder was 3: 1(molar ratio). The Fritsch Pulverisette-4 planetary ball mill produced by the German company Fritsch was used to mill the powder for 6 hours to uniformly mix the powder.

Table 2. Chemical composition of Stellite 12 powder (wt %)

Fe	C	Si	Mn	W	Mo	Cr	Ni	Co
1.99	1.34	1.27	0.11	7.92	0.14	30.43	2.34	Bal.

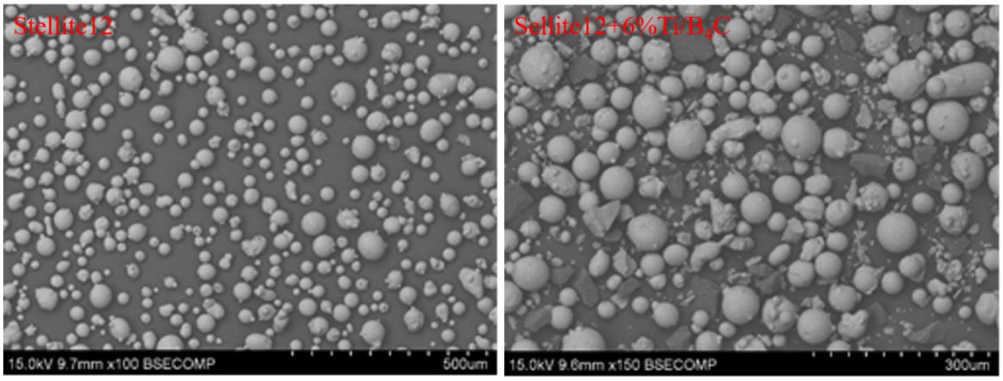

Fig. 1 Morphology of pure Stellite12 and Stellite12+6% Ti/B_4C powder

Fig. 1 shows the morphologies of pure stellite12 powder and stellite12+6% Ti/B_4C powder. It can be seen that the particle size of stellite12 powder is 75μm, and the particle sizes of Ti and B_4C added are about 30-75μm.

2.2Methods

Laser cladding was conducted in the argon shielded chamber of a 5 kW fiber laser material processing system (IPG YLS-5000, IPG Photonics, Boston, MA, USA) and the spot diameter is 5.0 mm. After grinding and polishing the cross section of the coating, it was corroded with aqua regia for 40 seconds. VHX-600K super depth of field microscope produced by Japan Keyence Corporation and S-4300N SEM produced by Hitachi Japan were used to observe the microstructure of the cladding layer. The energy spectrum analysis (EDS) included in the SEM was used for energy spectrum analysis. The XPERT-PRO type polycrystalline XRD produced by Panac Corporation was used for phase analysis. HXD-1000 Vickers micro hardness tester produced by Shanghai Taiming Optical Instrument Co., Ltd. was used to measure the hardness of the coatings from the surface to the substrate in the vertical direction of the cross section. The weight of the load was 200 gram-force and the holding time was 15 seconds. The lap area was cut into a size of 10 mm×10 mm×10 mm, and polished for friction and wear experiments. The friction and wear test adopted the CFT-1 material surface comprehensive tester produced by Lanzhou Zhongke Kaihua technology development co. LTD., using Si_3N_4 as the friction pair material, the load was 50N, the wear speed was 0.1m / s, and the test time was 30 minutes. And the effect of Ti/B_4C on the oxidation resistance of Stellite 12 powder coating was studied. The coating was cut into 10 mm×6 mm×1 mm and for the oxidation test. The surface of the specimen were ground by abrasive papers of #150, #400, #800, #1200 to make sure the surface smooth. The isothermal oxidation test was conducted in a muffale furnace at 800℃ for 50 h. The specimens were brought out once every two hours to weigh the mass by an analytical balance with the accuracy of 0.1 mg.

This article uses a preset powder. The laser power was 2000 W and the scanning was 1000 mm / min.

3. Results and discussion

3.1 Analysis of XRD results of coatings

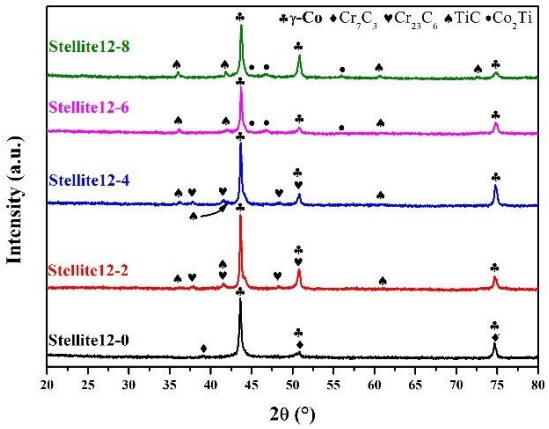

Fig. 2 XRD patterns of the coatings

From the results in Fig. 2, when the powder was pure Stellite 12 powder, the products were mainly γ-Co and Cr_7C_3, etc. When Ti/B_4C with 2%, and 4% mass fractions was added, the main phases in the coating were γ-Co, TiC and $Cr_{23}C_6$. And when Ti/B_4C with 6%, and 8% mass fractions was added, the main phases in the coating were γ-Co, TiC and Co_2Ti. It can observe that γ-Co was the main component phase of each coating. The reason for this is that laser cladding is a rapid melting and nonequilibrium solidification process. γ-Co produced at high temperatures had solidified without transformation[18]. In addition, the solid solution of Fe and Ni in the coating will reduce the phase transition temperature. This was conducive to the formation of the γ-Co phase. In Stellite 12 powder, the content of Cr was second only to Co. Cr was mainly present as Cr carbides (Cr_7C_3 and $Cr_{23}C_6$) in the coating. Other trace amounts of W, Fe, and Ni in the powder were mainly present as solid solutions. The results showed that with the increase of Ti/B_4C in the coating, a hard TiC phase was produced and gradually increased. Because the binding capacity of Ti to B is stronger than that of Ti to C. So Ti and C form the TiC phase and gradually increase. At the same time, when the Ti/B_4C doping content was 6% and 8%, the Co_2Ti phase appeared.

3.2 Analysis of coating structure and morphology

3.2.1 Macromorphology

It is worth mentioning that experiments with higher Ti/B_4C doping ratio were also performed. 10% and 12% Ti/B_4C + stellite 12 coatings were also prepared on 304 substrates.

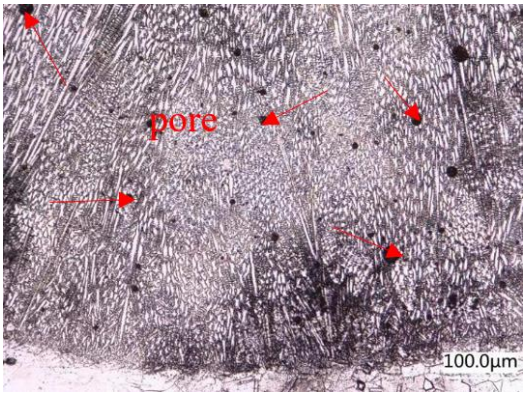

Fig. 3 Microstructure of stellite 12 + 10% Ti/B_4C coatings.

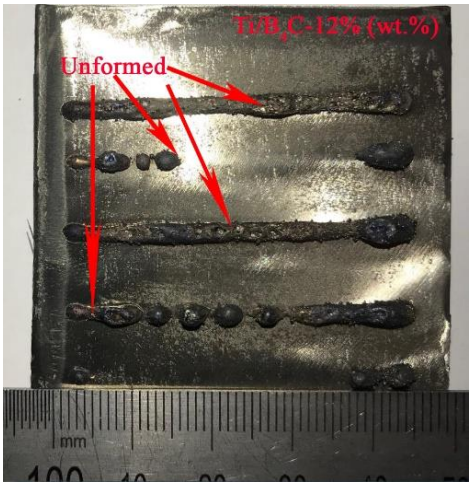

Fig. 4 Macromorphology of stellite 12 + 12% Ti/B_4C coatings.

Fig. 3 is the morphology of stellite12 + 10% Ti/B_4C coatings. It can be seen that a large number of pores were presented in the coating. Because under the same process parameters, the more Ti/B_4C content, the higher the laser energy required in the laser cladding process. The melting of the powder generates a large amount of gas before it overflows and exists in the coating, forming a large number of pores. Fig. 4 was the macro morphology of stellite12 + 12% Ti/B_4C coatings. It can be seen that the laser energy was seriously insufficient, the powder was not fully melted, the coating was not formed. So the addition of Ti/B_4C goes up to 8%.

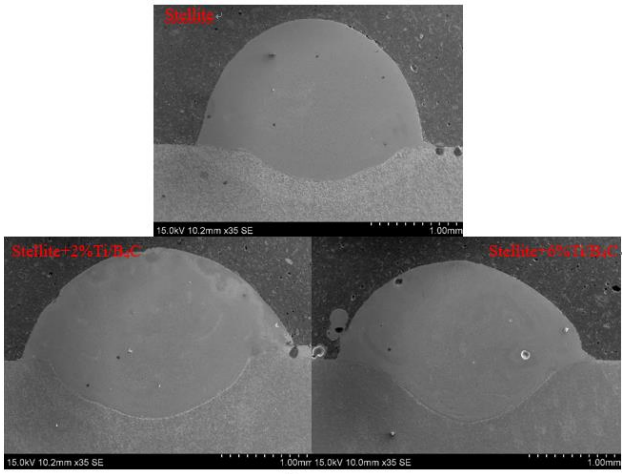

Fig. 5 Stelliet 12 adds 0%, 2%, 6% Ti/B_4C coating cross-section

Fig. 5 indicates the macroscopic morphology in the cross section of coating. It can be seen from Fig. 5, the coating is metallurgically bonded well to the substrate and possesses dense microstructure without any microcracks and pores. The addition of Ti/B_4C of different quantities had a certain effect on the combination of substrate and coating. There were obvious changes in the molten pool. Compared to the Stellite 12 coating, the doped coatings had wider melt width and deeper penetration. Due to the addition of Ti/B_4C, the absorption of laser energy by the coating in the laser cladding process was increased, which was reflected in the macroscopic aspect that the width and depth of the coating become larger.[19]

3.2.2 Microstructure analysis

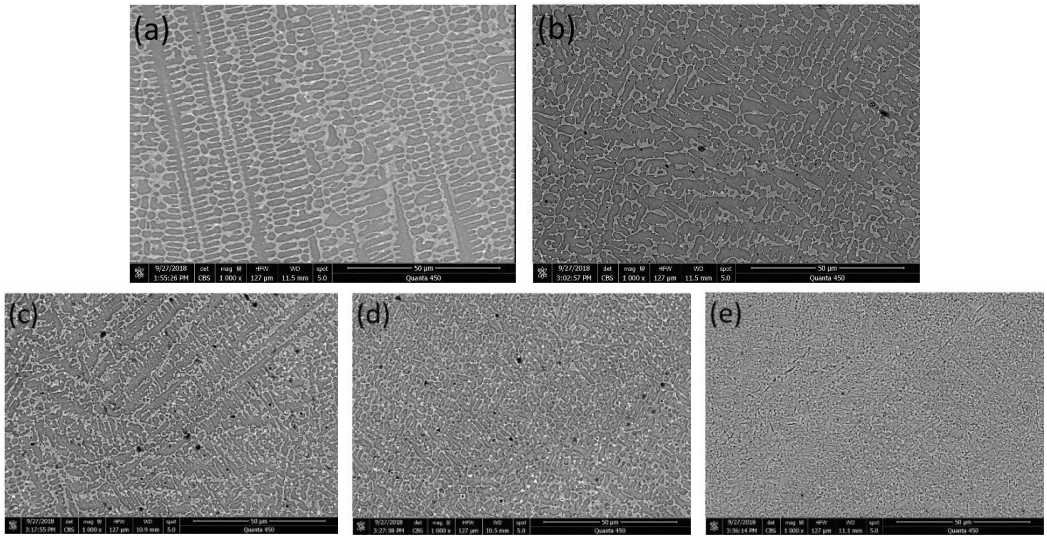

Fig. 6 Microstructural characteristics of （a）Stellite 12 coating（b）Stellite 12+2%Ti/B_4C coating（c）Stellite 12+4%Ti/B_4C coating（d）Stellite 12+6%Ti/B_4C coating（e）Stellite 12+8%Ti/B_4C coating

It can be seen from Fig. 6, the five coatings were possessed dense microstructure without any microcracks and pores. In Fig. 6(a), the substrate coating mainly grew in the shape of dendrite, and the growth direction of the dendrites had a certain angular

relationship with the interface. The main reason was the crystal anisotropy and the direction of heat flow during the dendrite growth. Fig. 6(b) shows 2% Ti/B_4C added, the growth of dendrites had changed significantly. A little equiaxed crystals appeared in the coating. It can be seen from Fig. 6(c)-(e), the dendrites gradually disappeared with the increase of Ti/B_4C content. At the same time, the coating structure was changed from dendrite to equiaxed crystal, and the coating structure was significantly refined.

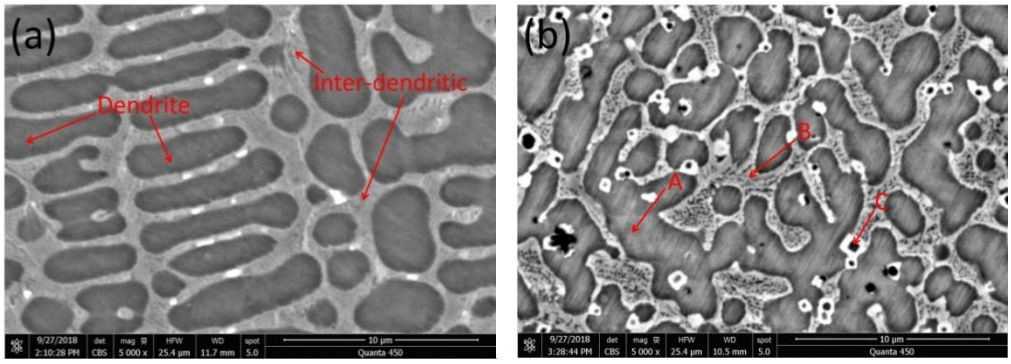

Fig. 7 Microstructures of phases in coatings: （a）Stellite 12（b）Stellite 12+6%Ti/B_4C

Table 3. EDS test results of coatings（at. %）

Zone	Co	Cr	W	Ni	Ti	B	C	Fe
dendrite	47.42	25.56	3.53	4.14	-	-	2.94	13.39
Inter-dendtitic	43.78	30.80	3.51	3.18	-	-	3.01	12.68
(A)	27.76	25.22	2.86	5.21	1.23	-	3.41	28.46
(B)	28.77	21.57	2.88	4.76	1.01	-	4.70	30.30
(C)	2.63	4.20	0.39	0.44	0.09	87.25	1.45	2.91

To identify the chemical constitutions of these phases in coatings, EDS was used and the result are listed in Table 3. Table 3 shows the EDS analysis results of the dendritic region and inter-dendrite region of the pure Stellite 12 powder coating and the dendritic region (A), inter-dendrite region (B) and black particle phase (C) of the 6% Ti/B_4C doped composite coating. According to the EDS results, it can be seen that compared with the pure Stellite 12 coating, the Fe content in the Ti/B_4C doped coating significantly increased. The main reason was that the addition of Ti/B_4C promoted the absorption of laser energy in the laser cladding process. The diffusion of Fe from base material to coating was promoted.[19] Combined with the XRD results, the dendrites of the pure Stellite 12 coating were mainly γ-Co primary dendrites. It was a solid solution with a large number of Cr and Fe elements. The inter-dendrite structure was a layered subeutectic structure with carbides contained Cr and other elements on the basis of γ-Co. According to the EDS results in Table 3, the results showed that in stellite 12+6%Ti/B_4C coatings, (A) and (B) had more Co, Cr and Fe elements and less Ti and C elements. There was a lot of B elements and a little bit of C elements at (C).

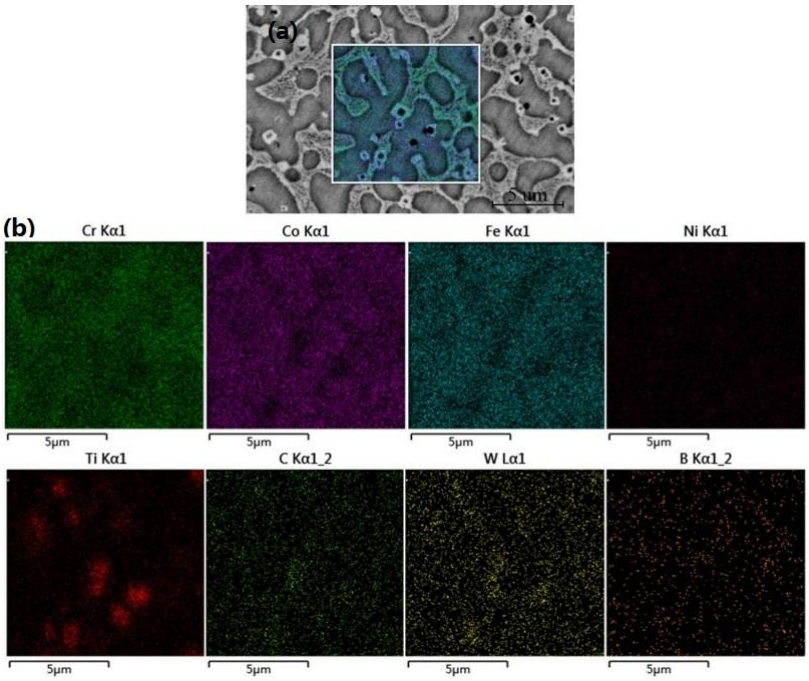

Fig. 8 SEM-EDS maps of Stellite 12+6%Ti/B_4C coating

Combined with XRD, EDS and the surface scanning results in Fig. 8, it was concluded that the white coated black particle phase in Fig. 7 (b) was composed of TiC and B_4C. And according to the principle of backscatter imaging (the lower the average atomic number, the darker the contrast, and the brighter the other way around)[20], it can be seen that the white phase was TiC and the black phase was B_4C. Similarly, it can be seen that the white bright spots between dendrites in Fig. 7 (a) were W. As Ti/B_4C was added, the hard phase TiC was generated in situ on the coating. And the remaining incompletely melted B_4C was used as the heterogeneous nucleation point. Therefore, it was observed that the TiC-encapsulated B_4C particle phase was dispersed in the coating. This particle played a dispersive strengthening role in the coating.

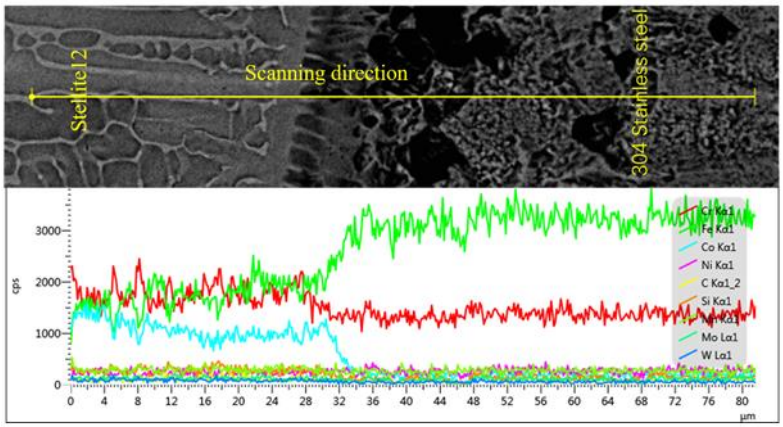

Fig. 9 Stellite 12 coating EDS linear scan results

Fig. 9 shows the EDS line scan results of stellite12 coating. The linear scan

results showed that the content of Fe element in the Stellite12 coating was also higher. Because of the base material melted during the laser cladding process, and the base material element Fe diffused into the coating. During the laser cladding process, because of the influence of heat, the metal flew in the molten pool, and the element Co of the coating diffused slightly to the 304 stainless steel. Meanwhile, the distribution of elements such as Cr, W, Mo and Ni was relatively uniform.

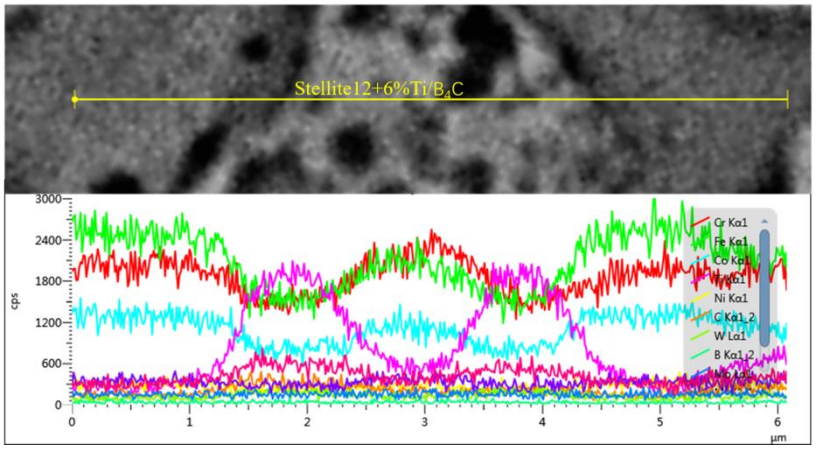

Fig. 10 Stellite 12+6%Ti/B_4C coating EDS line scan results

In order to analyze the diffusion of elements in the coating after Ti/B_4C was added, EDS line scan analysis was performed for typical tissues of Stellite 12 with 6%Ti/B_4C doped. From the results of line scan analysis in Fig. 10, it can be seen that the elements such as Co, Cr, and Fe were evenly distributed, and a large number of Ti elements existed in the coating. Combined with the XRD result, adding Ti/B_4C generated the hard phase TiC in situ.

The secondary dendrite arm spacing of pure Stellite 12 dendrites was about 2.346 μm. The distances between the secondary dendrite arms were: 2.312 μm (2% Ti/B_4C), 1.755 μm (4% Ti/B_4C), 1.525 μm (6% Ti/B_4C), and 1.500 μm (8% Ti/B_4C). At the beginning, because of the small amount of added Ti/B_4C, the nucleation of γ-Co could not be fully inhibited, and the growth mode of dendrites did not change significantly. When the Ti/B_4C content more than 2%, the secondary dendrite arms were significantly reduced. When 8%Ti/B_4C was added, the spacing between secondary dendrite arms were three-fifths of that without addition. According to the results of the XRD, with the increase of the content of Ti/B_4C, the hard TiC phases in the coating gradually increased. These hard phases played a role of hardening the grains and promoted the crystal grain refinement during solidification process.

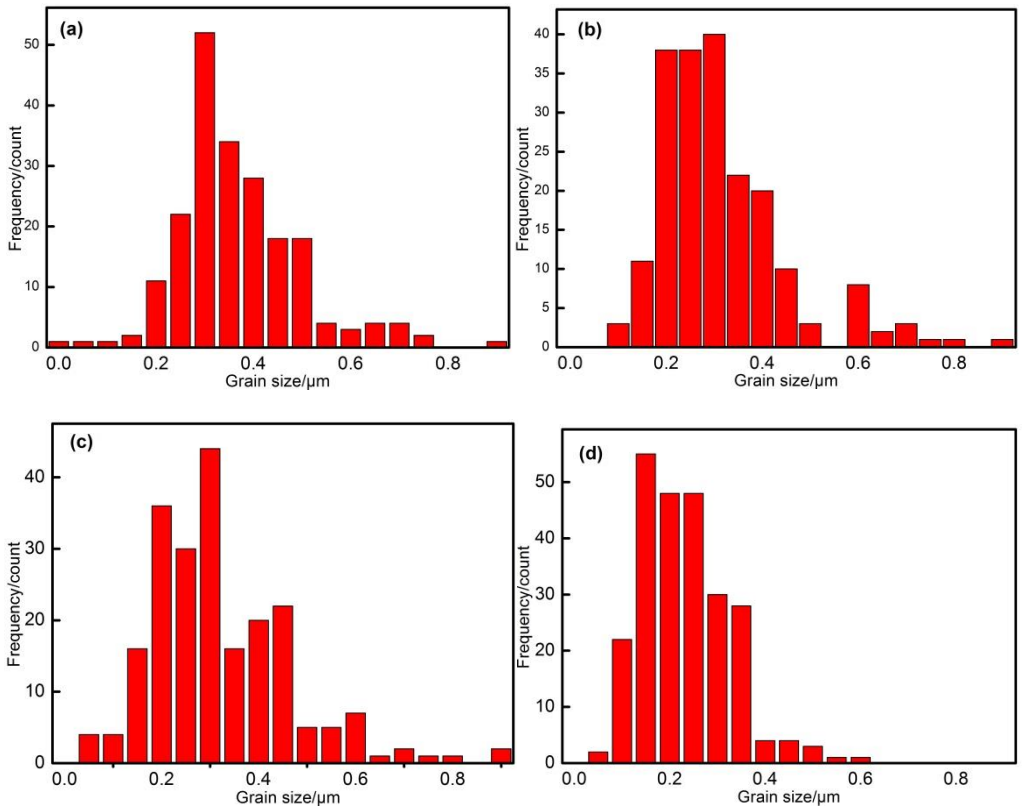

Fig. 11 Frequency counts of grain size（a）Stellite 12+2%Ti/B_4C（b）Stellite 12+4%Ti/B_4C

（c）Stellite 12+6%Ti/B_4C（d）Stellite 12+8%Ti/B_4C

Fig. 11 shows the frequency distribution diagram of grain phase size (Dendrite and isometric crystal) in Fig. 6 (b)-(e). From Fig. 11 (a), it can be seen that the grain phase size of the coating doped with 2% Ti/B_4C ranged from 0.25 to 0.55 μm. However, from Fig. 11 (b), the results showed that the grain phase size of the coating doped with 4% Ti/B_4C ranged from 0.15 to 0.50 μm. From Fig. 11 (c), the results showed that the grain phase size of the coating doped with 6% Ti/B_4C ranged from 0.15 to 0.545 μm. From Fig. 11 (d), the results showed that the grain phase size of the coating doped with 8% Ti/B_4C ranged from 0.15 to 0.40 μm. From these results, it can be seen that the coating grain is obviously refined. The size range of B_4C particles in the original powder was 30 to 75 μm. During the rapid melted and solidification process of laser cladding, the B_4C submicrometer phase still existed. The TiC formed in situ took B_4C as the nucleate particle. Therefore, the grain size of the grain phase depended on the size of the remained B_4C particles. With the increase of Ti and B_4C in the coating, the laser absorptivity of the coating gradually increased. This leads to a reduction in the size of the residual B_4C. Therefore, the size of TiC (particle phase with B_4C as nucleation particle) decreased and remained at the submicron level.

3.3 Analysis of coating mechanical properties

3.3.1 Microhardness of the coating

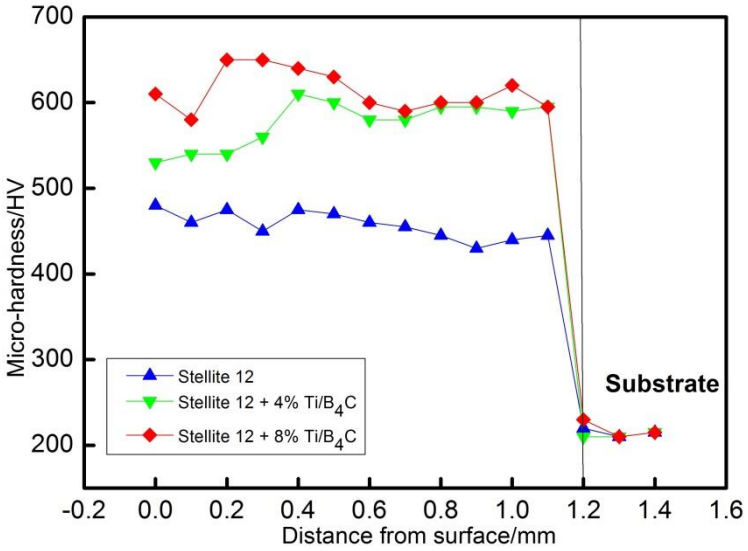

Fig. 12 Microhardness curve of the coatings along the depth

Fig. 12 shows the microhardness distribution of the cladding coatings along the depth. It can be seen that the microhardness of the coatings was distinctly different with the different contents of Ti/B_4C. It may be attributed to the microstructural variations and the constitutions. Judging from the Fig. 12, the results can be drawn that a transition point existed between the substrate and cladding coatings and the value of microhardness of the coating near the substrate declines remarkedly. This was mainly owed to the coating diluted by the substrate. The average microhardness of the coatings were 457 HV, 576HV, 614HV. The highest microhardness was 650HV. Compared with 304 stainless steel substrate (220HV), the microhardness of each coating had been improved. With the increase of Ti/B_4C content in Stellite 12, the microhardness of the coating was improved. When Ti/B_4C was 8%, the microhardness of the coating was almost three times than that of 304 stainless steel. On the one hand, adding Ti/B_4C can reduce the secondary dendrite arms spacing of the structure, refine the structure and improve the performance; On the other hand, the Ti/B_4C submicron particle phase dispersed in the coating can play a significant role in dispersion and strengthening, and both can jointly improve the microhardness of the coating.

3.3.2 Wear resistance of coating

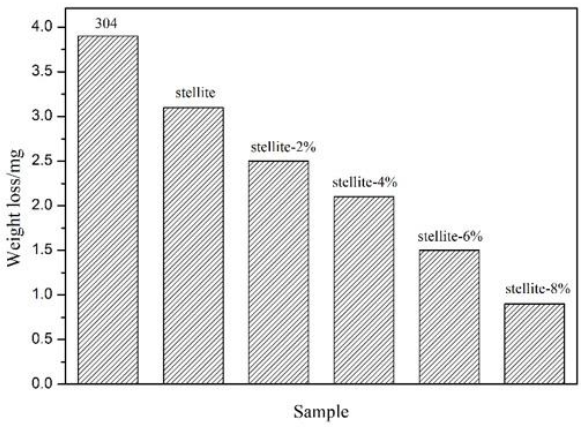

Fig. 13 Comparison of wear resistance of 304 stainless steel substrate and each deposited coating

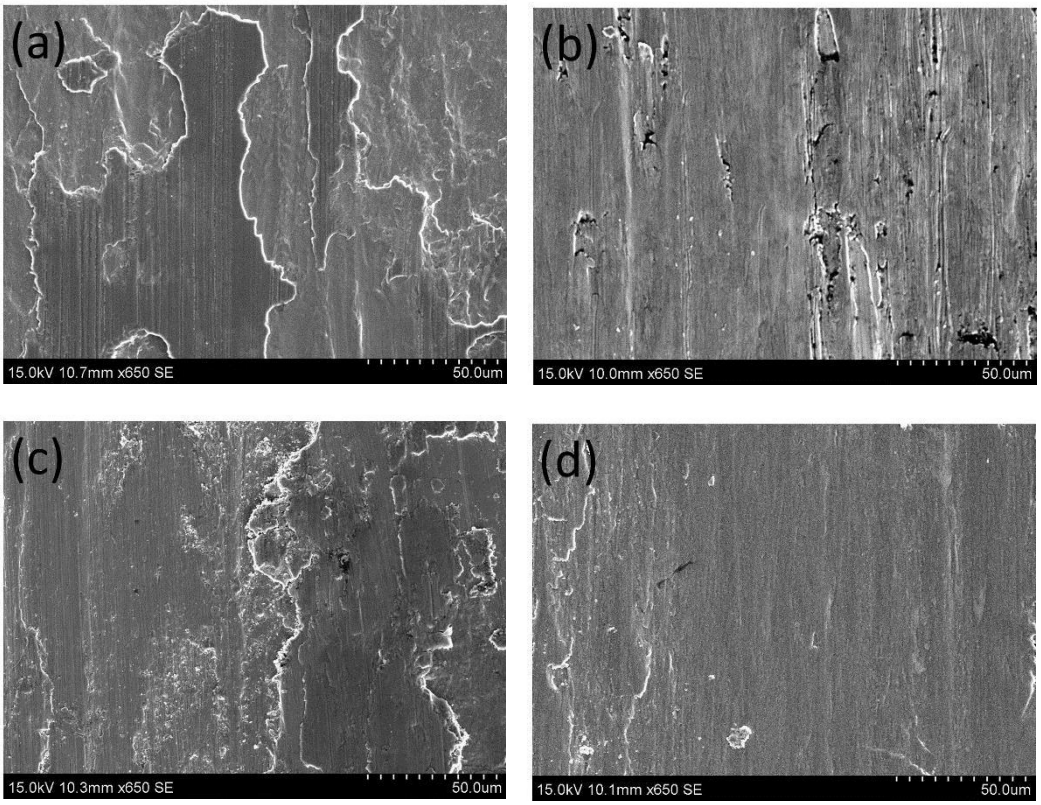

Fig. 14 Worn surface morphologies of （a）304 Stainless Steel Substrate（b）Stellite 12 coating （c）Stellite 12+4%Ti/B_4C coating（d）Stellite 12+8%Ti/B_4C coating

Fig. 13 shows the comparison of wear resistance of base material and different coatings. From the analysis of friction and wear, it can be concluded that the wear resistance of the cladding coating on the 304 stainless steel substrate had been significantly improved. When the addition amount was 0% Ti/B_4C, 2% Ti/B_4C, 4% Ti/ B_4C, 6% Ti/B_4C, 8% Ti/B_4C, it can be seen that the effect of different content Ti/ B_4C on the wear resistance of Stellite 12 coating. With the increase of Ti/B_4C doping, the wear resistance of the coating became better. With the increase of Ti/B_4C content, the dispersed TiC/B_4C hard particle phase had a good anti-wear effect. And the morphology of the structure gradually changed from dendrites to equiaxed crystals. An equiaxed polycrystalline array was gradually formed in the tissue. Under the external force of sliding friction, the polycrystalline grains can achieve mutual coordination and hinder dislocation movement. Improved the deformation resistance and hindered the development of cracks, and improved the wear resistance of the coating[21]. Through sliding friction and wear experiments, the average friction coefficients of 304 stainless steel substrate, Stellite 12+0% Ti/B_4C, Stellite 12+4% Ti/B_4C, and Stellite 12+8% Ti/B_4C were: 0.62, 0.55, 0.47, and 0.41, respectively. It can be known from the friction coefficient that the external addition of Ti/B_4C had improved the abrasion resistance of the coating.

To characterize the morphologies of the worn surfaces of the substrate and the coatings, SEM observation was carried out on the samples. As shown in Fig. 14(a),

the substrate presents severe adhesive and abrasive wear due to the serious plastic deformation, deep plowing grooves and flaking debris. As shown in Fig. 14(b), the wear pattern of pure Stellite 12 coating is mainly furrows, and the wear resistance was improved compared with 304 stainless steel substrates. As shown in Fig. 14(c), the wear resistance of the coating was enhanced, and the main wear form was abrasive wear. When 4%Ti/B_4C was added, the coating contained the hard phase TiC and partially melted B_4C. Due to the presence of the high hardness TiC phase, the wear resistance of the coating was improved. As shown in Fig. 14(d), when 8% Ti/B_4C was added, the wear morphology of the coating was relatively smooth and slightly of furrows for abrasive wear. In summary, when the Ti/B_4C content was 8%, the wear resistance of the Stellite 12 coating was best.

3.3.3 Study on high temperature oxidation of coatings

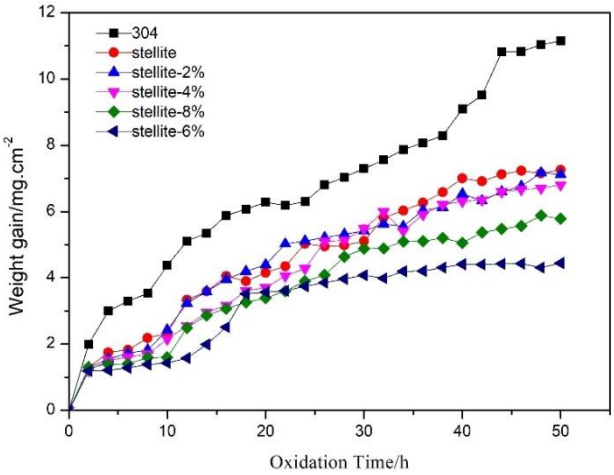

Fig. 15 Oxidation weight gain curve of the substrate and cladding coatings at 800 °C for 50 h

Fig. 15 presents the oxidation weight gain curves of the substrate and cladding coating exposed 800℃ for 50 h. Obviously, the weight of all the samples had a growing tendency with the elongation of oxidation time. In addition, the weight gain of coatings is clearly lower than that of the substrate at the same temperature during the oxidation. With the increase of Ti/B_4C, the weight gain of the coating was also different, showed a downward trend. When the addition amount of Ti/B_4C was 6%, the increase of the weight was the least. It also had the lowest growth rate. The results showed that Stellite 12 coating had certain temperature oxidation resistance on the substrate. And the addition of Ti/B_4C to Stellite 12 can improve the oxidation resistance at high temperature. According to all the data in Fig. 15, it can be seen that the high temperature oxidation process of each composite coating could be roughly divided into rapid oxidation and relatively stable oxidation stages, whose change form was a parabola. It can be seen from the literature that if the oxidation kinetics curves of metals and alloys conform to parabolic laws, they will have good oxidation resistance. In the rapid oxidation stage, because of the coating was in direct contact with oxygen, the reaction was rapid in the high temperature environment, producing a large number of oxides, resulting in rapid weight gain. With the formation of oxides, the coating surface was covered by the generated oxides, or oxide film, which

prevented further contact with oxygen, thus reducing the production of oxides and reducing the weight of oxides.

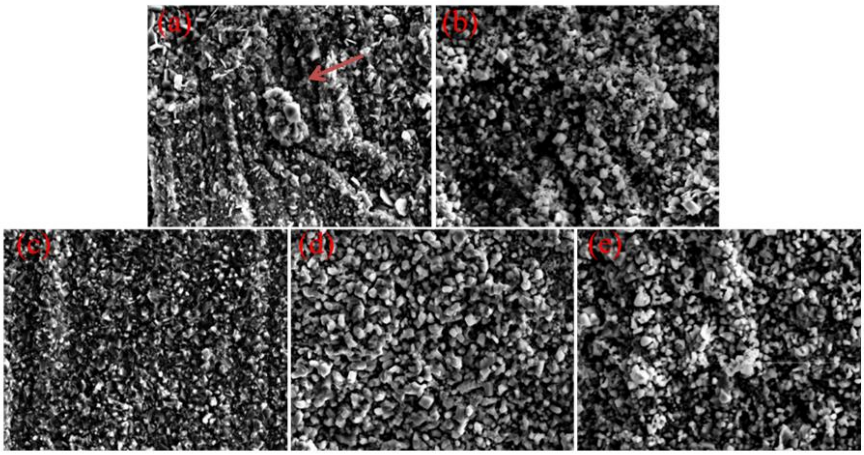

Fig. 16 SEM morphology of the cladding coating after 50 h high temperature oxidation (a) Stellite 12 coating (b) stelite 12+ 2% Ti/B_4C coating (c) stelite 12+ 4% Ti/B_4C coating (d) stelite 12+ 6% Ti/B_4C coating (e)stelite 12+8%Ti/B_4C coating

It can be seen that the morphology of each coating after high temperature oxidation is different. Fig. 16(a) shows the morphology of pure Stellite 12 coating after high temperature oxidation. There was a large amount of oxide with large size on the surface, but there was also the phenomenon of oxide film peeling. The direction of the red arrow is one of the places where the oxide film falls off. The reason for falling off was that the thermal expansion coefficient of the coating material and the oxide was different, and the coating surface appeared cracks and falls off. [22] Fig. 16 (b, c, d, e) shows the morphology after high temperature oxidation with 2% - 8% Ti/B_4C doped. It can be seen from the Fig. 16(b)-(e), the oxide size was smaller and denser than that of the pure Stellite 12 coating, which was why the addition of Ti/B_4C had better resistance to high temperature oxidation of the coating. The results showed that the oxide coating was the densest when the addition of Ti/B_4C was 6%. According to the literature, grain refinement can improve the toughness of the oxide film, and the plastic deformation of the oxide film can release the stress accumulated in the coating, thus improving the adhesion of the oxide film. [23] Therefore, when the content of Ti/B_4C increased, the coating grain got smaller, and the adhesion of the oxide layer got higher, the oxidation resistance of the coating got better.

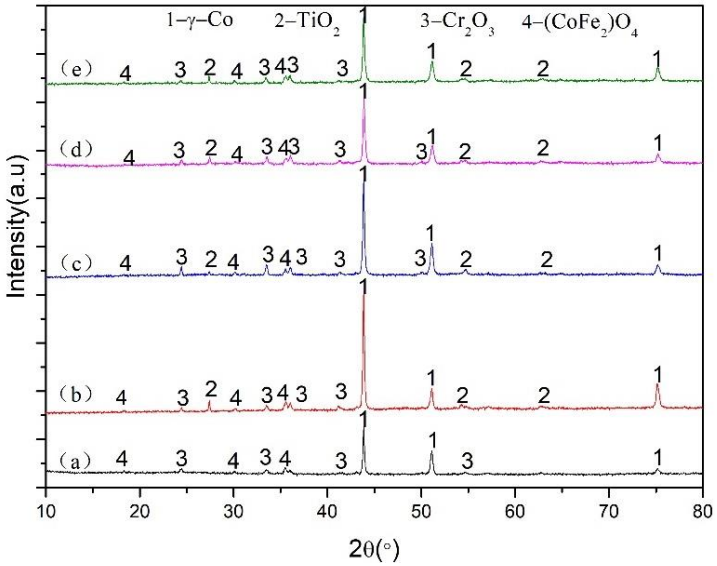

Fig.17 XRD patterns of the cladding coating after high temperature oxidation for 50 h (a) Stellite 12 coating (b) stelite 12+ 2% Ti/B_4C coating (c) stelite 12+ 4% Ti/B_4C coating (d) stelite 12+ 6% Ti/B_4C coating (e)stelite 12+8%Ti/B_4C coating

Fig. 17 (a) shows the XRD patterns of pure Stellite 12 coating after high temperature oxidation for 50h. It can be concluded that the phases of pure Stellite 12 after high temperature oxidation were mainly γ-Co, Cr_2O_3 and $(CoFe_2)O_4$. When different ratios of Ti/B_4C were added, the phases after high temperature oxidation resistance were not much different. The main phases were γ-Co, Cr_2O_3, $(CoFe_2)O_4$, and TiO_2. TiO_2 was formed because the added Ti was oxidized at high temperature. The results showed that, compared with stellite 12 coating, because of TiO_2 oxidation film was formed on the coating, the oxidation resistance of the coating was improved.[24], [25] But when Ti/B_4C content was 8%, its oxidation resistance was weaker than the coating with Ti/B_4C content of 6%. Therefore, the increase of antioxidant capacity had nothing to do with the increase of Ti content. When Ti content was too high, too much TiO_2 was produced, and the oxide film became loose and porous, thus causing the oxide film to fall off.

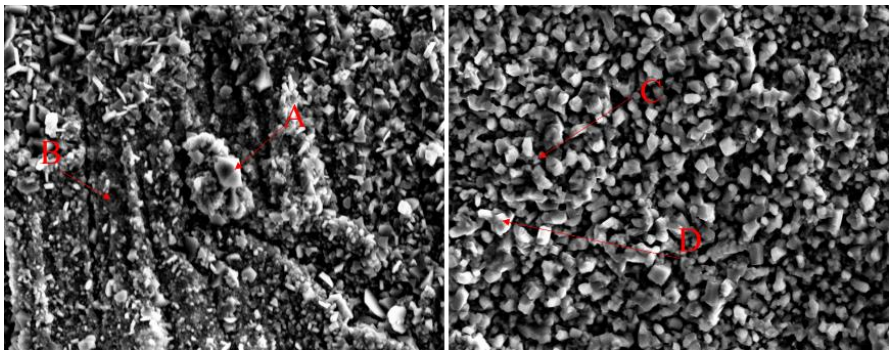

Fig. 18 Typical morphology of Stellite 12 coating and stelite 12+6%Ti/B_4C coating after high temperature oxidation for 50h

Table 4. Analysis of fixed-point components of high temperature oxidation EDS

for Stellite and stelite+6% Ti/B_4C coatings

Regions	O	Cr	Ti	Fe	Co
A	25.82	58.42	-	1.55	-
B	24.34	56.65	-	6.25	-
C	27.56	6.18	59.18	1.83	0.74
D	23.11	7.09	61.51	1.88	0.75

In order to further analyze the chemical composition of the oxide layer, an EDS analysis was performed on the oxide layer. Point A and point B of pure Stellite 12 coating after high temperature oxidation and point C and point D of stelite 12+6%Ti/B_4C coating after high temperature oxidation were analyzed by EDS fixed-point energy spectrum analysis, and the results are shown in Table 4. From the elements of A and B, it was known that the pure stelite12 coating oxidized to the oxides of Fe and Cr after high temperature oxidation, and there were relatively few Co oxides on the surface of the coating. It was known from the literature that when the temperature was heated below 850 ℃ for a short time, the alloying element Cr in the coating reacted with oxygen to form Cr_2O_3 first. Because of the high stability of Co, it was not easy to form oxides at 800 ℃. It can be known from the elements of C and D that after adding Ti/B_4C, the coating contained not only Cr, Co, O, but also Ti element after high temperature oxidation. Combined with the XRD analysis results, it can be known that the phase of pure Stellite 12 coating after high temperature oxidation were γ-Co, Cr_2O_3, $(CoFe_2)$ O_4. And $(CoFe_2)$ O_4 was speculated that the Fe element in Fe_3O_4 is replaced by Co. After Ti/B_4C was added, the phases of the coating were γ-Co, Cr_2O_3, $(CoFe_2)$ O_4 and TiO_2 after high temperature oxidation.

4. Conclusion

1、A well-formed Stellite 12 and Ti/B_4C composite coating was obtained by laser cladding, and the coating formed well without obvious defects. The coating phases with 2% and 4% Ti/B_4C were mainly γ-Co, $Cr_{23}C_6$ and TiC, and the coating phases with 6% and 8% Ti/B_4C were mainly γ-Co, Co_2Ti and TiC

2、With the addition of Ti/B_4C, the secondary dendrite arms spacing of the coating dendrite gradually became smaller, and the coating grains gradually became finer. And coating grains were submicron.

3、With the addition of Ti/B_4C, the hardness and wear resistance of the coating had been improved. When the added Ti/B_4C was 8%, the performance was optimal. The average hardness value was 624HV and the average coefficient of friction was 0.41.

4、The high temperature oxidation resistance of the composite coating on the substrate had increased. After adding Ti/B_4C, the oxidation resistance of the coating had been improved. When the Ti/B_4C was 6%, the coating had the highest high temperature oxidation resistance.

Acknowledgements

This research was supported by Natural Science Foundation of China (51605276, 51905333), Shanghai Sailing Program (19YF1418100), Shanghai Science and Technology Committee Innovation Grant (17JC1400600, 17JC1400601, 19511106400, 19511106402), Karamay Science and Technology Major Project (2018ZD002B), Aid for Xinjiang Science and Technology Project (2019E0235), Shanghai Local Colleges and Universities Capacity Building Special Plan Project (19030501300).

References

[1] A. Gholipour, M. Shamanian, and F. Ashrafizadeh, “Microstructure and wear behavior of stellite 6 cladding on 17-4 PH stainless steel,” *J. Alloys Compd.*, vol. 509, no. 14, pp. 4905–4909, 2011, doi: 10.1016/j.jallcom.2010.09.216.

[2] A. Kusmoko, D. Dunne, and H. Li, “Effect of Heat Input on Stellite 6 Coatings on a Medium Carbon Steel Substrate by Laser Cladding,” *Mater. Today Proc.*, vol. 2, no. 4–5, pp. 1747–1754, 2015, doi: 10.1016/j.matpr.2015.07.010.

[3] F. Arias-González *et al.*, “Fiber laser cladding of nickel-based alloy on cast iron,” *Appl. Surf. Sci.*, vol. 374, pp. 197–205, 2016, doi: 10.1016/j.apsusc.2015.11.023.

[4] F. Weng, C. Chen, and H. Yu, “Research status of laser cladding on titanium and its alloys: A review,” *Mater. Des.*, vol. 58, pp. 412–425, 2014, doi: 10.1016/j.matdes.2014.01.077.

[5] M. J. Tobar, J. M. Amado, A. Yáñez, J. C. Pereira, and V. Amigó, “Laser cladding of MCrAlY coatings on stainless steel,” *Phys. Procedia*, vol. 56, no. C, pp. 276–283, 2014, doi: 10.1016/j.phpro.2014.08.172.

[6] C. T. Kwok, H. C. Man, and F. T. Cheng, “Cavitation erosion and pitting corrosion of laser surface melted stainless steels,” *Surf. Coatings Technol.*, vol. 99, no. 3, pp. 295–304, 1998, doi: 10.1016/S0257-8972(97)00624-5.

[7] Q. Y. Pan, W. D. Huang, R. G. Song, Y. H. Zhou, and G. L. Zhang, “The improvement of localized corrosion resistance in sensitized stainless steel by laser surface remelting,” *Surf. Coatings Technol.*, vol. 102, no. 3, pp. 245–255, 1998, doi: 10.1016/S0257-8972(98)00358-2.

[8] Y. Yang, Z. P. Jiang, and H. Z. Li, “Effect of Co - Based Alloy on Properties of Laser Cladding Layer,” *IOP Conf. Ser. Mater. Sci. Eng.*, vol. 265, no. 1, 2017, doi: 10.1088/1757-899X/265/1/012021.

[9] A. Motallebzadeh, E. Atar, and H. Cimenoglu, “Sliding wear characteristics of molybdenum containing Stellite 12 coating at elevated temperatures,” *Tribol. Int.*, vol. 91, pp. 40–47, 2015, doi: 10.1016/j.triboint.2015.06.006.

[10] V. V. Diaz, J. C. Dutra, and A. S. C. M. D’Oliveira, “Hardfacing by plasma transfer arc process,” *Weld. Int.*, vol. 26, no. 2, pp. 87–95, 2012, doi: 10.1080/09507116.2010.527486.

[11] V. Kuzucu, M. Ceylan, H. Çelik, and I. Aksoy, “An investigation of stellite-6 alloy containing 5.0 wt% silicon,” *J. Mater. Process. Technol.*, vol. 79, no. 1–3, pp. 47–51, 1998, doi: 10.1016/S0924-0136(97)00452-4.

[12] S. Kapoor, *High-Temperature Hardness and Wear Resistance of Stellite Alloys*, vol. 6, no. 7. 2012.

[13] A. Shahroozi, A. Afsari, and B. Khakan, “Microstructure and mechanical properties investigation of stellite 6 and Stellite 6/TiC coating on ASTM A105 steel produced by TIG welding process,” *Surf. Coatings Technol.*, vol. 350, pp. 648–658, 2018, doi: 10.1016/j.surfcoat.2018.07.044.

[14] Z. Y. Zhu, C. Ouyang, J. H. Chen, and Y. X. Qiao, “Microstructure and mechanical properties of stellite 6 alloy powders incorporated with Ti/B4C

using Plasma-Arc-surfacing processes," *Mater. Tehnol.*, vol. 53, no. 1, pp. 3–8, 2019, doi: 10.17222/MIT.2018.044.

[15] B. Du, S. R. Paital, and N. B. Dahotre, "Synthesis of TiB 2-TiC/Fe nano-composite coating by laser surface engineering," *Opt. Laser Technol.*, vol. 45, no. 1, pp. 647–653, 2013, doi: 10.1016/j.optlastec.2012.05.017.

[16] H. Deng, H. Shi, and S. Tsuruoka, "Influence of coating thickness and temperature on mechanical properties of steel deposited with Co-based alloy hardfacing coating," *Surf. Coatings Technol.*, vol. 204, no. 23, pp. 3927–3934, 2010, doi: 10.1016/j.surfcoat.2010.05.013.

[17] S. A. A. Dilawary, A. Motallebzadeh, R. Akhter, E. Atar, and H. Cimenoglu, "Enhanced wear resistance of Stellite 12 by Mo addition and LSM*," *Surf. Eng.*, vol. 34, no. 8, pp. 569–576, 2018, doi: 10.1080/02670844.2017.1393164.

[18] S. A. A. Dilawary, A. Motallebzadeh, A. H. Paksoy, M. Afzal, E. Atar, and H. Cimenoglu, "Influence of laser surface melting on the characteristics of Stellite 12 plasma transferred arc hardfacing deposit," *Surf. Coatings Technol.*, vol. 317, pp. 110–116, 2017, doi: 10.1016/j.surfcoat.2017.03.051.

[19] H. Qiao, Q. T. Li, H. G. Fu, and Y. P. Lei, "Microstructure and micro-hardness of in situ synthesized TiC particles reinforced Fe-based alloy composite coating by laser cladding," *Materwiss. Werksttech.*, vol. 45, no. 2, pp. 85–90, 2014, doi: 10.1002/mawe.201400188.

[20] Z. Peilei *et al.*, "Microstructure and wear behavior of Cu-Mo-Si coatings by laser cladding," *Appl. Surf. Sci.*, vol. 311, pp. 709–714, 2014, doi: 10.1016/j.apsusc.2014.05.141.

[21] L. F. Ganzales and I. N. Shiganov, "Optimization of the process of deposition of wear-resisting Stellite coatings on steel by laser radiation," *Weld. Int.*, vol. 32, no. 1, pp. 34–39, 2018, doi: 10.1080/09507116.2017.1369069.

[22] M. Kemdehoundja, J. F. Dinhut, J. L. Grosseau-Poussard, and M. Jeannin, "High temperature oxidation of Ni70Cr30 alloy: Determination of oxidation kinetics and stress evolution in chromia layers by Raman spectroscopy," *Mater. Sci. Eng. A*, vol. 435–436, pp. 666–671, 2006, doi: 10.1016/j.msea.2006.07.083.

[23] B. Gorr *et al.*, "High-temperature oxidation behavior of Mo-Si-B-based and Co-Re-Cr-based alloys," *Intermetallics*, vol. 48, pp. 34–43, 2014, doi: 10.1016/j.intermet.2013.10.008.

[24] M. Fadavi, A. R. Baboukani, H. Edris, and M. Salehi, "Study on high-temperature oxidation behaviors of plasma-sprayed TiB2-Co composite coatings," *J. Korean Ceram. Soc.*, vol. 55, no. 2, pp. 178–184, 2018, doi: 10.4191/kcers.2018.55.2.11.

[25] N. Jegadeeswaran, M. R. Ramesh, S. Prakrathi, and K. U. Bhat, "Hot corrosion behaviour of HVOF sprayed stellite-6 coatings on gas turbine alloys," *Trans. Indian Inst. Met.*, vol. 67, no. 1, pp. 87–93, 2014, doi: 10.1007/s12666-013-0317-z.